2008

A Mathematical Model for a Lithium–Sulfur Cell

Karthikeyan Kumaresan

Yuriy Mikhaylik

Ralph E. White
University of South Carolina - Columbia, white@cec.sc.edu

Publication Info

Published in *Journal of the Electrochemical Society*, Volume 155, Issue 8, 2008, pages A576-A582.

Journal of The Electrochemical Society, **155** (8) A576-A582 (2008)
0013-4651/2008/155(8)/A576/7/$23.00 © The Electrochemical Society

A Mathematical Model for a Lithium–Sulfur Cell

Karthikeyan Kumaresan,[a,*] Yuriy Mikhaylik,[b,] and Ralph E. White[a,***,z]**

[a]*Department of Chemical Engineering, University of South Carolina, Columbia, South Carolina 29208, USA*
[b]*Sion Power Corporation, Tucson, Arizona 85706-7129, USA*

A mathematical model is presented for a complete lithium–sulfur cell. The model includes various electrochemical and chemical (precipitation) reactions, multicomponent transport phenomena in the electrolyte, and the charge transfer within and between solid and liquid phases. A change in the porosity of the porous cathode and separator due to precipitation reactions is also included in the model. The model is used to explain the physical reasons for the two-stage discharge profiles that are typically obtained for lithium–sulfur cells.
 [DOI: 10.1149/1.2937304]

Manuscript submitted February 5, 2008; revised manuscript received May 7, 2008. Available electronically June 18, 2008.

The lithium/sulfur cell is a promising energy storage system due to its high theoretical specific energy density (2600 Wh/kg), good low-temperature performance, and inexpensive and nontoxic raw materials. Earlier studies[1,2] of the electrochemical reduction of sulfur in various electrolytes based on aprotic solvents indicate that elemental sulfur in solution ($S_{8(l)}$) is reduced to S^{2-} in steps. For example, ($S_{8(l)}$) is reduced to S_8^{2-}, then to S_6^{2-}, S_4^{2-}, S_2^{2-}, and finally to S^{2-} during discharge. But the exact number of stable intermediate sulfide ions during the discharge of a lithium/sulfur cell has not yet been identified beyond doubt. A number of different organic solvents have been used by various research groups[3-8] studying the lithium/sulfur cell. The solubility of these intermediate sulfide ions depends on the solvent used in the electrolyte, and hence the voltage vs discharge capacity profile of the cell depends on the solvents used. For example, solvents like tetrahydrofuran and dimethyl sulfoxide can dissolve considerably larger quantities of longer polysulfides, and the discharge profiles of the cells with electrolytes based on these solvents show two distinct stages.[3,4] Figure 1 presents a typical experimental discharge profile at a C/50 rate (C = 2.5 Ah). The lithium/sulfur cell used to obtain the above discharge profile was made with a composite sulfur cathode (solid elemental sulfur, conductive carbon, and a binder), metallic lithium foil anode, and a proprietary electrolyte. The discharge profile consists of two distinct stages separated by a local voltage minimum, the first stage between 2.45 and 2.1 V, where the voltage drop is significant, and the second stage, where the voltage remains relatively constant. A complete understanding of the discharge profile presented in Fig. 1 requires an in-depth analysis of the complex interaction between the electrochemical reactions like lithium oxidation on the anode and reduction of various sulfides in the cathode and chemical reactions consisting of precipitation/dissolution of elemental sulfur and various solid lithium sulfide species. A mathematical model of a lithium/sulfur cell is presented in this paper to aid such an analysis. The model can be used to analyze the effect of various parameters associated with the electrochemical reactions, chemical reactions, and transport phenomena on the discharge behavior of the lithium/sulfur cell.

Model Development

The schematic of the lithium/sulfur cell modeled in this work is shown in Fig. 2. The cell is made up of a metallic lithium anode foil and a porous-carbon, sulfur cathode separated by a porous separator.

Reactions in the cell.— At the anode surface, lithium metal is oxidized to Li^+ during discharge

$$\mathrm{Li} \underset{\mathrm{d}}{\overset{\mathrm{c}}{\rightleftarrows}} \mathrm{Li}^+ + \mathrm{e}^- \quad [1]$$

During discharge, the elemental sulfur in the solid phase ($S_{8(s)}$) in the cathode is first dissolved in the electrolyte as $S_{8(l)}$ and then reduced to sulfide ions with progressively lower states of oxidation according to the following electrochemical reactions

$$\frac{1}{2}\mathrm{S}_{8(l)} + \mathrm{e}^- \underset{\mathrm{c}}{\overset{\mathrm{d}}{\rightleftarrows}} \frac{1}{2}\mathrm{S}_8^{2-} \quad [2]$$

$$\frac{3}{2}\mathrm{S}_8^{2-} + \mathrm{e}^- \underset{\mathrm{c}}{\overset{\mathrm{d}}{\rightleftarrows}} 2\mathrm{S}_6^{2-} \quad [3]$$

$$\mathrm{S}_6^{2-} + \mathrm{e}^- \underset{\mathrm{c}}{\overset{\mathrm{d}}{\rightleftarrows}} \frac{3}{2}\mathrm{S}_4^{2-} \quad [4]$$

$$\frac{1}{2}\mathrm{S}_4^{2-} + \mathrm{e}^- \underset{\mathrm{c}}{\overset{\mathrm{d}}{\rightleftarrows}} \mathrm{S}_2^{2-} \quad [5]$$

$$\frac{1}{2}\mathrm{S}_2^{2-} + \mathrm{e}^- \underset{\mathrm{c}}{\overset{\mathrm{d}}{\rightleftarrows}} \mathrm{S}^{2-} \quad [6]$$

In addition to the above electrochemical reactions in the cathode, chemical precipitation/dissolution reactions also occur during the discharge process. At the beginning of the discharge most of the elemental sulfur is in the solid phase ($S_{8(s)}$) due to its low solubility value (19 mol/m^3). As the elemental sulfur in the liquid phase ($S_{8(l)}$) is consumed by the electrochemical reduction reaction (Eq. 2) during the discharge, the concentration of the soluble sulfur ($S_{8(l)}$) drops below its equilibrium solubility limit. This causes dissolution of solid elemental sulfur into the liquid phase as given by

$$\mathrm{S}_{8(l)} \rightleftharpoons \mathrm{S}_{8(s)} \quad [7]$$

As the discharge proceeds, the concentrations of Li^+ ions and sulfide ions increase. Depending on the local concentrations of Li^+ ions and individual sulfide ions, one or more of the following precipitates may be formed: $Li_2S_{8(s)}$, $Li_2S_{6(s)}$, $Li_2S_{4(s)}$, $Li_2S_{2(s)}$, or $Li_2S_{(s)}$. But, previous experimental studies indicate that all lithium sulfides except $Li_2S_{2(s)}$ and $Li_2S_{(s)}$ are substantially soluble[6] in the electrolyte. In addition to precipitation of $Li_2S_{2(s)}$ and $Li_2S_{(s)}$, the model also includes the precipitation of $Li_2S_{8(s)}$ and $Li_2S_{4(s)}$ for illustration purposes. The precipitation/dissolution reactions are assumed to occur according to the following equations

$$2\mathrm{Li}^+ + \mathrm{S}_8^{2-} \rightleftharpoons \mathrm{Li}_2\mathrm{S}_{8(s)} \quad [8]$$

$$2\mathrm{Li}^+ + \mathrm{S}_4^{2-} \rightleftharpoons \mathrm{Li}_2\mathrm{S}_{4(s)} \quad [9]$$

$$2\mathrm{Li}^+ + \mathrm{S}_2^{2-} \rightleftharpoons \mathrm{Li}_2\mathrm{S}_{2(s)} \quad [10]$$

* Electrochemical Society Student Member.
** Electrochemical Society Active Member.
*** Electrochemical Society Fellow.
z E-mail: white@engr.sc.edu

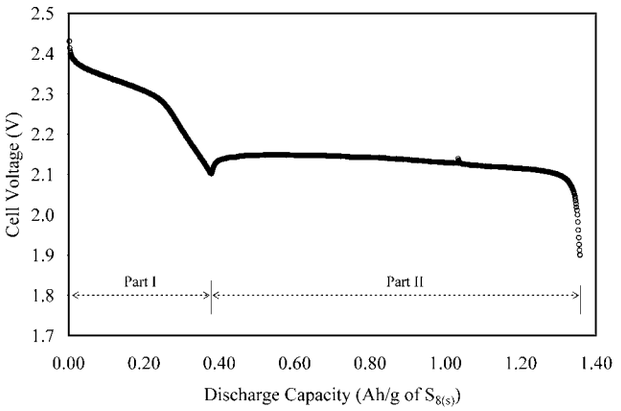

Figure 1. Room-temperature experimental C/50 rate (C = 2.5 Ah) discharge profile.

$$2Li^+ + S^{2-} \rightleftharpoons Li_2S_{(s)} \quad [11]$$

Governing Equations

For a multicomponent electrolyte system in a porous medium, the material balance on an individual species is given by[9]

$$\frac{\partial\, \varepsilon C_i}{\partial\, t} = -\ \nabla\ \cdot N_i + r_i - R_i \quad [12]$$

where ε represents the pore volume fraction of the porous cathode or separator, and C_i is the concentration of species i ($i = Li^+$, $S_{8(l)}$, S_8^{2-}, S_6^{2-}, S_4^{2-}, S_2^{2-}, S^{2-}, and A^-). Here A^- denotes the anion of the lithium salt used in the electrolyte. The flux of the species i, N_i, which is due to both diffusion and migration, can be written for a dilute solution as follows

$$\frac{N_i}{\varepsilon} = -\ D_i\ \nabla\ C_i - z_i \frac{D_i}{RT} F C_i\ \nabla\ \phi_2 \quad [13]$$

where D_i is the diffusion coefficient of species i, corrected for porosity and tortuosity using the Bruggeman expression ($D_i = D_{i,o}\varepsilon^b$, $D_{i,o}$ is the diffusion coefficient in bulk medium, and b is the Bruggeman coefficient accounting for the porosity and tortuosity of the porous separator and cathode), z_i is the charge number of species i, and ϕ_2 is the liquid-phase potential. The second term on the right side of Eq. 12, r_i, is the rate of production (or consumption, if negative) of species i by all of the electrochemical reactions in which species i participates and can be related to the current densities due to each of the electrochemical reactions as follows

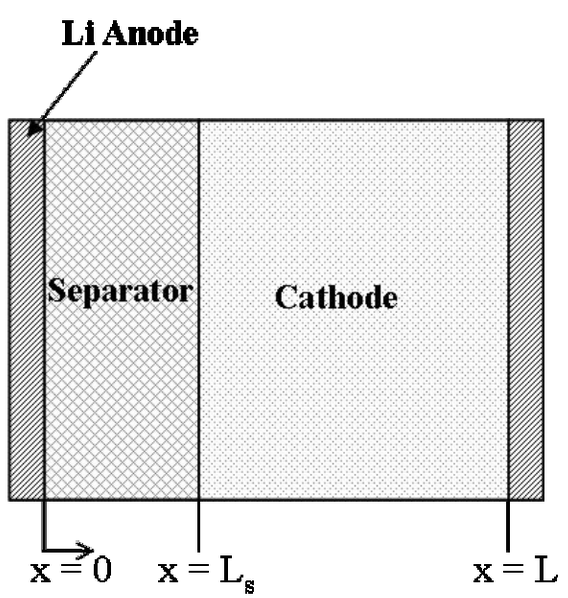

Figure 2. Schematic of lithium–sulfur cell.

Table I. Stoichiometric coefficients, $s_{i,j}$.

	Reactions given by equation, j $s_{i,j}$					
Species, i	1	2	3	4	5	6
Li^+	−1	0	0	0	0	0
$S_{8(l)}$	0	−1/2	0	0	0	0
S_8^{2-}	0	1/2	−3/2	0	0	0
S_6^{2-}	0	0	2	−1	0	0
S_4^{2-}	0	0	0	3/2	−1/2	0
S_2^{2-}	0	0	0	0	1	−1/2
S^{2-}	0	0	0	0	0	1
A^-	0	0	0	0	0	0

$$r_i = -\ a \sum_j \frac{s_{i,j} i_j}{n_j F} \quad [14]$$

where a denotes the specific area of the porous cathode, which is defined as the area of solid/liquid interface per unit volume of the porous medium (separator or cathode), n_j denotes the number of electrons transferred in reaction j, and $s_{i,j}$ is the stoichiometric coefficient of species i in electrochemical reaction j written in the following form

$$\sum_i s_{i,j} M_i^{z_i} = n_j e^- \quad [15]$$

The precipitation of various lithium sulfides in the cathode decreases the electrochemically active interfacial area between the solid and liquid phases. Consequently, it is assumed in this model that the specific surface area of the cathode varies according to the following empirical expression

$$a = a_o \left(\frac{\varepsilon}{\varepsilon_{initial}} \right)^{\xi} \quad [16]$$

where ξ is the empirical parameter describing the morphology of the precipitate and is assigned a value of 1.5 in this work. A list of the stoichiometric coefficients of species in reactions given by Eq. 1-6 is given in Table I. The current density due to the electrochemical reaction j at the solid/liquid interface is given by the Butler–Volmer equation in the following form[10]

$$i_j = i_{o,jref} \left\{ \prod_i \left(\frac{C_i}{C_{i,ref}} \right)^{p_{i,j}} \exp\left(\frac{\alpha_{aj} F}{RT} \eta_j \right) - \prod_i \left(\frac{C_i}{C_{i,ref}} \right)^{q_{i,j}} \times \exp\left(-\ \frac{\alpha_{cj} F}{RT} \eta_j \right) \right\} \quad [17]$$

where the overpotential for reaction j is given by

$$\eta_j = \phi_1 - \phi_2 - U_{j,ref} \quad [18]$$

and

$$p_{i,j} = s_{i,j} \quad \text{(for anodic species)} \quad [19]$$

$$q_{i,j} = -\ s_{i,j} \quad \text{(for cathodic species)} \quad [20]$$

The open-circuit potential (OCP) for reaction j at the reference concentrations $C_{i,ref}$ (assumed to be equal to initial concentration) of species i is given by

$$U_{j,ref} = U_j^{\theta} - \frac{RT}{n_j F}\sum_i s_{i,j} \ln\left[\frac{C_{i,ref}}{1000}\right] \quad [21]$$

Because Eq. 21 is valid only when the concentrations are expressed in moles per liter, reference concentrations are divided by the factor 1000 in order to convert their units from moles per meter cubed to moles per liter. The liquid-phase current density, i_e, is related to the liquid-phase potential and the liquid-phase concentrations by

$$i_e = F\sum_i z_i N_i \quad [22]$$

The solid-phase charge transfer is purely by electronic conduction. So, it can be defined by the conventional Ohm's law

$$i_s = -\sigma \nabla \phi_1 \quad [23]$$

The following equation is required to place the constraint that the charge can enter or leave the liquid phase only by the electrochemical reaction at the solid/liquid interface in the cathode

$$\nabla \cdot i_e = a\sum_j i_j \quad [24]$$

Finally, charge is conserved in the porous medium as stated in Eq. 25 below, which says that the charge leaving a phase must be equal and opposite of the charge entering the other phase

$$\nabla \cdot i_s + \nabla \cdot i_e = 0 \quad [25]$$

The third term on the right side of Eq. 12, R_i, is the rate of production or consumption of species i due to precipitation/dissolution reactions, which can be related to the rate of precipitation/dissolution reaction k by

$$R_i = \sum_k \gamma_{i,k} R'_k \quad [26]$$

where R'_k is the rate of precipitation of the solid species k ($S_{8(s)}$, $Li_2S_{8(s)}$, $Li_2S_{4(s)}$, $Li_2S_{2(s)}$, $Li_2S_{(s)}$) and $\gamma_{i,k}$ is the number of moles of ionic species i in the solid species k. The rate of precipitation of species k, assuming that the precipitation reaction is kinetically controlled can be written as

$$R'_k = k_k \varepsilon_k \left(\prod_i C_i^{\gamma_{i,k}} - K_{sp,k}\right) \quad [27]$$

In the above equation, $K_{sp,k}$ is the solubility product of k in the electrolyte and k_k is the rate constant. Apart from the supersaturation (term enclosed by parenthesis), Eq. 27 includes the fact that the rate of precipitation of species k depends on the solid volume fraction of the precipitate k (ε_k) in order to account for the slow rate of nucleation at the beginning of the precipitation reaction. At the beginning of the discharge, the volume fraction of each of the four lithium sulfide precipitates ($Li_2S_{8(s)}$, $Li_2S_{4(s)}$, $Li_2S_{2(s)}$, and $Li_2S_{(s)}$) is zero. During discharge, once the electrolyte becomes supersaturated with a given sulfide ion (e.g., S^{2-}) the precipitation of corresponding lithium sulfide (e.g., $Li_2S_{(s)}$) begins. The first step of the precipitation reaction is nucleation, where a discrete number of nuclei are formed at the active sites of the porous separator and cathode. Further precipitation occurs at the interface between these nuclei and the liquid phase, resulting in the growth of nuclei to form particles of precipitate. So, during the early stages of the precipitation process, the rate of precipitation depends on both the number of nuclei and the interfacial area between the nuclei and the liquid phase.[11] For a precipitate of constant density, the interfacial area can be assumed to be directly proportional to its volume fraction, and hence the rate of precipitation is assumed to depend on the volume fraction of the precipitate in Eq. 27.

The porosity of the porous (ε) cathode increases with the dissolution of solid elemental sulfur ($S_{8(s)}$) and decreases when one or more of the lithium sulfide species precipitates. Using the rate of precipitation R'_k and the partial molar volume $\tilde{V}_k$ ($k = S_{8(s)}$, $Li_2S_{8(s)}$, $Li_2S_{4(s)}$, $Li_2S_{2(s)}$, and $Li_2S_{(s)}$) of the precipitates, the variation of porosity of the cathode (and separator) with time can be expressed as

$$\frac{\partial \varepsilon}{\partial t} = -\sum_k \tilde{V}_k R'_k \quad [28]$$

The volume fraction of precipitate k ($k = S_{8(s)}$, $Li_2S_{8(s)}$, $Li_2S_{4(s)}$, $Li_2S_{2(s)}$, $Li_2S_{(s)}$) can be expressed as a function of time as given below

$$\frac{\partial \varepsilon_k}{\partial t} = \tilde{V}_k R'_k \quad [29]$$

Boundary Conditions

At the cathode/current collector interface ($x = L$).— Ten boundary conditions are needed at $x = L$ (eight for the species concentrations and one each for ϕ_1 and ϕ_2). Due to the presence of the cathode current collector (a physical barrier), the flux of each species i ($i = Li^+$, $S_{8(l)}$, S_8^{2-}, S_6^{2-}, S_4^{2-}, S_2^{2-}, S^{2-}, and A^-) is set equal to zero at this boundary

$$N_i = 0 \text{ at } x = L \quad [30]$$

Moreover, at this boundary all the current density is carried by the solid phase and it is equal to the external current density applied to the cell. This means that the solution-phase current density at this boundary is zero

$$-\sigma \nabla \phi_1 = I_{app} \quad \text{at } x = L \quad [31]$$

$$i_e = 0 \quad \text{at } x = L \quad [32]$$

At the separator/cathode interface ($x = L_s$).— Because there are 10 differential equations on either side of this interface, 10 boundary conditions are required. At the separator/cathode interface, the flux of each of the eight species is continuous, which can be expressed mathematically as

$$N_{i,separator} = N_{i,cathode} \quad \text{at } x = L_s, \quad [33]$$

At this interface all the current is carried by solution phase alone. It can also be said that at this interface the solution-phase current density on the separator side equals that in the cathode side, i.e., the solution-phase current density is continuous through the interface. Moreover, the solid-phase current density at this point is zero

$$i_{e,separator} = i_{e,cathode} \quad \text{at } x = L_s \quad [34]$$

and

$$-\sigma \nabla \phi_1 = 0 \quad \text{at } x = L_s \quad [35]$$

Anode/separator interface ($x = 0$).— At this boundary 10 boundary conditions are required as there are 10 differential equations in the separator region. Because Li^+ is the only reacting species at the anode/separator interface (in the absence of side reactions), the flux of all species except Li^+ ($i = S_{8(l)}$, S_8^{2-}, S_6^{2-}, S_4^{2-}, S_2^{2-}, S^{2-}, and A^-) is set equal to zero

$$N_i = 0 \quad \text{at } x = 0 \quad [36]$$

The flux boundary condition of the concentration of Li^+ can be written as

$$N_1 = \frac{i_1}{F} \quad \text{at } x = 0 \quad [37]$$

where i_1 is the surface current density on the anode, which is given by the Butler–Volmer relation given by Eq. 17. The solid-phase potential at this point is set to be equal to 0 in order to have a reference point for the potential. Mathematically, this can be written as

Table II. Kinetic and thermodynamic properties.

Reaction (j)	$i_{o,jref}$[a] (A/m^2)	α_{aj}	α_{cj}	n_j	$U_j^{\theta a}$ (V)
1	0.394	0.5	0.5	1	0.0
2	1.972	0.5	0.5	1	2.39
3	0.019	0.5	0.5	1	2.37
4	0.019	0.5	0.5	1	2.24
5	1.97×10^{-4}	0.5	0.5	1	2.04
6	1.97×10^{-7}	0.5	0.5	1	2.01

[a] Assumed parameters.

$$\phi_1 = 0 \quad \text{at } x = 0 \qquad [38]$$

Because the only species with nonzero flux at this boundary is Li^+, the liquid-phase current density at $x = 0$ is given by

$$i_e = FN_1 \quad \text{at } x = 0 \qquad [39]$$

The governing equations (Eq. 28 and 29) describing the solid volume fractions (ε_k) and the pore volume fraction (ε) are ordinary differential equations in time; consequently, boundary conditions are not needed for these variables. The parameters used in the model are given in Tables II-V. The reference concentrations of all the species given in Table III are equal to the respective initial concentrations. The governing equations were solved numerically using COMSOL Multiphysics, which uses the finite element method to discretize the governing equations.

Table III. Transport properties and reference concentrations.

Species (i)	z_i	D_{io}[a] (m^2/s)	$C_{i,ref}$ (mol/m^3)
Li^+	+1	1×10^{-10}	1001.04
$S_{8(l)}$	0	1×10^{-9}	19.0[a]
S_8^{2-}	−2	6×10^{-10}	0.178[b]
S_6^{2-}	−2	6×10^{-10}	0.324[b]
S_4^{2-}	−2	1×10^{-10}	0.020[b]
S_2^{2-}	−2	1×10^{-10}	5.229×10^{-7} [b]
S^{2-}	−2	1×10^{-10}	8.267×10^{-10} [b]
A^-	−1	4×10^{-10}	1000.0[a]

[a] Assumed parameters.
[b] Calculated based on the assumed standard OCPs.

Table IV. Separator and cathode parameters.

Parameter	Separator[a]	Cathode[a]
Thickness (m)	9×10^{-6}	41×10^{-6}
$\varepsilon_{initial}$	0.37	0.778
$\varepsilon_{S_{8(s)},initial}$	1×10^{-12}	0.160
$\varepsilon_{Li_2S_{8(s)},initial}$	1×10^{-6}	1×10^{-6}
$\varepsilon_{Li_2S_{4(s)},initial}$	1×10^{-6}	1×10^{-6}
$\varepsilon_{Li_2S_{2(s)},initial}$	1×10^{-6}	1×10^{-6}
$\varepsilon_{Li_2S_{(s)},initial}$	1×10^{-7}	1×10^{-7}
a_o (m^2/m^3)	—	132,762
b	1.5	1.5

[a] Assumed parameters.

Results and Discussion

The concentration profiles of the Li^+ ions across the thickness of the cell at various times during a constant current ($0.394\ A/m^2$) discharge rate are shown in Fig. 3a. The concentration of Li^+, which is $1001.04\ mol/m^3$ (Table III) at the beginning of the discharge, increases during the first 14 h of discharge and then decreases with further discharge. The reason for such a behavior exhibited by the Li^+ concentration is that during the initial period of discharge (up to 14 h) S_8^{2-}, S_6^{2-}, and S_4^{2-} are the sulfide ions that are predominantly produced, through reactions given by Eq. 2-4, respectively, in the cathode. As the solubility values of the above sulfide ions are high, these sulfide ions do not precipitate, and their concentrations in the electrolyte increase. Consequently, the Li^+ ions produced from the anode during this stage of the discharge process also remain in the electrolyte, thus increasing its concentration. As the discharge proceeds further, the cell voltage decreases and the reactions given by Eq. 5 and 6, whose standard OCPs are significantly lower, become predominant, producing $S_2^{2-}$and S^{2-}. This results in the lowering of the concentrations of S_8^{2-}, S_6^{2-}, and S_4^{2-} ions in the electrolyte. Figure 3b shows that the concentration of S_4^{2-} ions increases to $\sim 1000\ mol/m^3$ at 14 h of discharge and it decreases with further discharge. The sulfide ions produced during later stages of the discharge, S_2^{2-} and S^{2-}, are only sparingly soluble in the electrolyte. So, as soon as the electrochemical production of S_2^{2-} and S^{2-} begins, the precipitation of either $Li_2S_{2(s)}$ or $Li_2S_{(s)}$ or both (depending on the relative values of their rate constants) begins. This is illustrated in Fig. 3c, where the variation of the concentration profiles of S^{2-} ions with discharge time is presented. The concentration of S^{2-} remains low during the first 14 h of discharge. Once the electrochemical production of S^{2-} begins, the electrolyte becomes supersaturated with S^{2-} ions. Because the precipitation reaction is kinetically controlled (once the nucleation phenomenon is complete, as discussed in more detail later) according to Eq. 27, the concentration of S^{2-} does not change significantly with time as long as the precipitation of $Li_2S_{(s)}$ occurs. As more and more soluble sulfides (S_8^{2-}, S_6^{2-}, and S_4^{2-}) are electrochemically reduced to sparingly soluble sulfides (S_2^{2-} and S^{2-}), the concentration of the Li^+ ion decreases as shown in Fig. 3a.

The concentration profiles of Li^+ do not show any significant gradients across the thickness of the cell at various stages of discharge. This is an expected trend because of the low rate of discharge. The S_4^{2-} concentration profile develops a negative gradient across the separator/cathode interface. This is because the rate of consumption of S_4^{2-} in the cathode (by the electrochemical reduction to S_2^{2-} and by the precipitation of $Li_2S_{4(s)}$) is slightly higher than the rate of S_4^{2-} transport from the separator to the cathode. In the case of S^{2-} ion, the rate of its accumulation (rate of electrochemical production of S^{2-} minus the rate of precipitation of $Li_2S_{(s)}$) is higher than

Table V. Parameters for precipitation reactions.

Precipitate (k)	Rate constant (k_k)[a]	Solubility product[a] (K_k)	Molar volume ($\tilde{V}_k$)[a] (m^3/mol)
$S_{8(s)}$	$1.0\ s^{-1}$	$19.0\ mol\ m^{-3}$	1.239×10^{-4}
$Li_2S_{8(s)}$	$1 \times 10^{-4}\ m^6\ mol^2\ s^{-1}$	$38.09\ mol^3\ m^{-9}$	1.361×10^{-4}
$Li_2S_{4(s)}$	$9.98 \times 10^{-5}\ m^6\ mol^2\ s^{-1}$	$11.26\ mol^3\ m^{-9}$	7.415×10^{-5}
$Li_2S_{2(s)}$	$9.98 \times 10^{-4}\ m^6\ mol^2\ s^{-1}$	$5.1 \times 10^{-3}\ mol^3\ m^{-9}$	4.317×10^{-5}
$Li_2S_{(s)}$	$27.5\ m^6\ mol^2\ s^{-1}$	$3.0 \times 10^{-5}\ mol^3\ m^{-9}$	2.768×10^{-5}

[a] Assumed parameters.

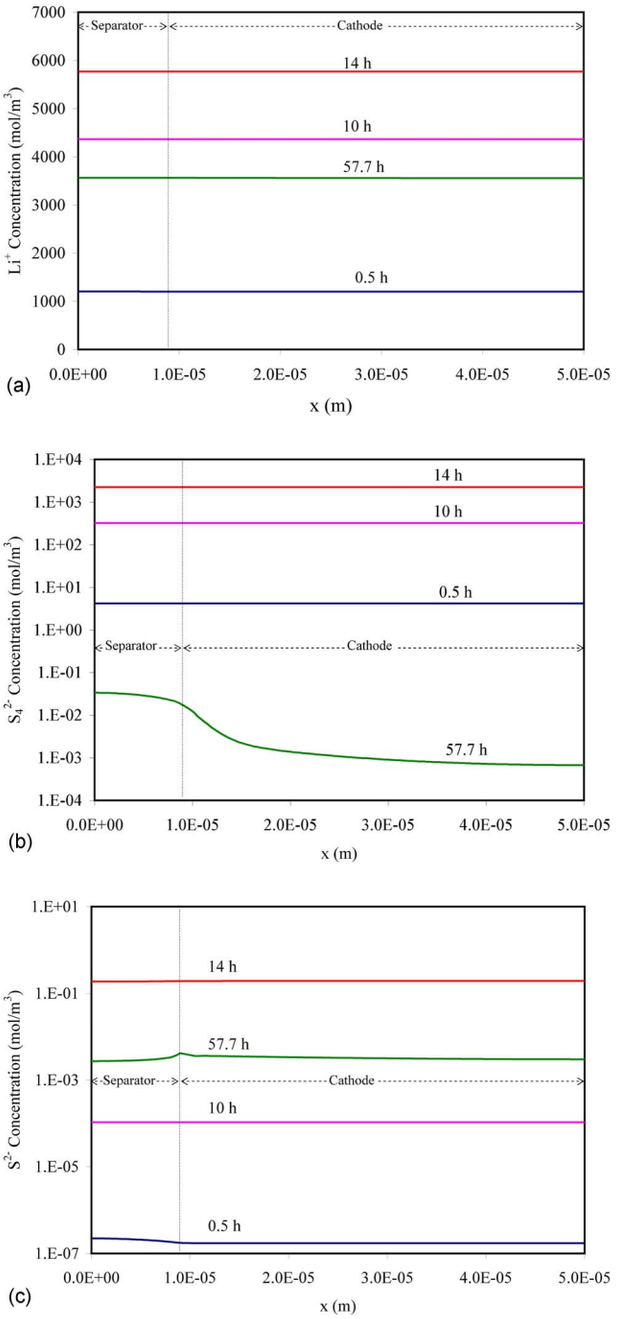

Figure 3. (Color online) Concentration profiles across the cell at different discharge times: (a) Li^+, (b) S_4^{2-}, and (c) S^{2-}.

the rate at which it is being transported to the separator. So, even at this low rate of discharge, the concentration profile of S^{2-} develops a positive gradient (Fig. 3c) in the separator near the separator/cathode interface.

The observed voltage vs time profile of the Li/S cell shown in Fig. 1 at a constant current is a result of different electrochemical and chemical (precipitation) reactions as mentioned above. An analysis of the variation of the concentration of all the reacting species with time provides us with further understanding about the reasons for shape of the discharge profile. The concentration of all the species varies with both time and space. But, as discussed earlier for the rate of discharge under consideration, the concentration of all the species have negligible gradient across the cathode. Even for the

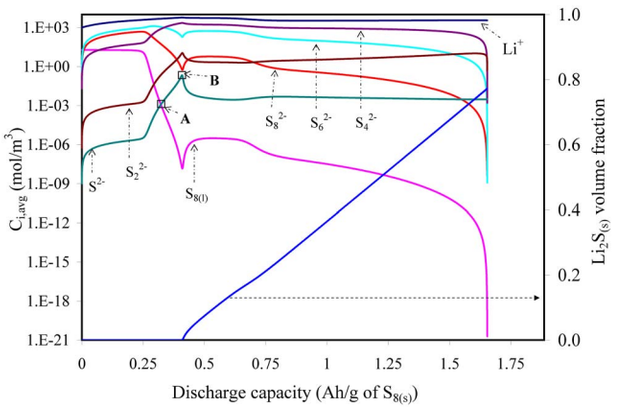

Figure 4. (Color online) Average concentrations ($C_{i,avg}$) and the average volume fraction of $Li_2S_{(s)}$ in the cathode as functions of discharge time.

precipitating species like S^{2-}, which develop concentration gradients in the separator region, the variation of concentration across the cathode is small at a given time. Therefore, the average concentrations of the sulfide species in the cathode calculated using the following expression are used for the rest of the analysis

$$C_{i,avg} = \frac{1}{(L - L_s)} \int_{x=L_s}^{x=L} C_i dx \qquad [40]$$

where $i = S_8$, S_8^{2-}, S_6^{2-}, S_4^{2-}, S_2^{2-}, S^{2-} as shown in Fig. 4. Because the concentration of Li^+ near the anode surface is more closely related to the cell voltage than that in the cathode, the average concentration for Li^+ ions is calculated across the separator. Based on the average concentrations vs discharge time profiles of reactive species presented in Fig. 4, the discharge process can be divided into two parts. During the first few hours of discharge, the dissolved elemental sulfur ($S_{8(l)}$) is reduced in the cathode, first to S_8^{2-} and then to S_6^{2-} and S_4^{2-}. The liquid phase is replenished with the elemental sulfur ($S_{8(l)}$) by the dissolution of elemental sulfur from the solid phase ($S_{8(s)}$). Because this dissolution process is kinetically controlled, the concentration of $S_{8(l)}$ remains at a constant value below its solubility limit (19 mol/m^3) until all of the elemental sulfur in the solid phase is dissolved completely. With further discharge, the concentration of $S_{8(l)}$ decreases, and so does the concentrations of S_8^{2-} and S_6^{2-}, as they are electrochemically reduced to S_4^{2-}. The rates of the reactions producing S_2^{2-} and S^{2-} (Eq. 5 and 6) become significant near the end of part I of the discharge. At point A (0.324 Ah/g of S_8) marked in Fig. 4, the ionic product $[Li^+]^2[S^{2-}]$ becomes larger than the solubility product K_{sp,Li_2S} and the precipitation of $Li_2S_{(s)}$ begins. Because no $Li_2S_{(s)}$ precipitate is present in the cathode at the beginning of the discharge, nucleation of the crystals occurs as a first step of precipitation. The precipitation is slow during the nucleation step, as its rate depends on the existing $Li_2S_{(s)}$ volume fraction as well as on the level of supersaturation according to Eq. 27. As a result of this, the level of supersaturation increases to a critical value at point B (0.409 Ah/g of S_8), and from there on the $Li_2S_{(s)}$ precipitation reaction becomes kinetically limited. From point B, the concentration of S^{2-} decreases to a lower value where it remains constant for the rest of the discharge period. The value of this constant S^{2-} concentration is determined by the relative rates of the electrochemical production of S^{2-} ions and the precipitation of S^{2-} ions as $Li_2S_{(s)}$. The higher the rate of precipitation, the lower the value concentration of S^{2-} in the low plateau region. The concentrations of S_6^{2-} and S_4^{2-} decrease gradually during part II of the discharge as they are reduced to S^{2-} and eventually precipitated as $Li_2S_{(s)}$.

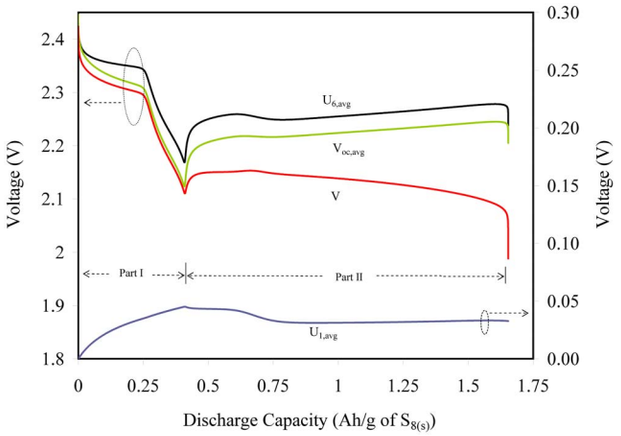

Figure 5. (Color online) Average OCPs of Li/Li$^+$ reaction ($U_{1,avg}$), S_2^{2-}/S^{2-} reaction ($U_{6,avg}$), and full-cell ($V_{oc,avg}$) and the simulated full cell voltage (V) as functions of discharge time.

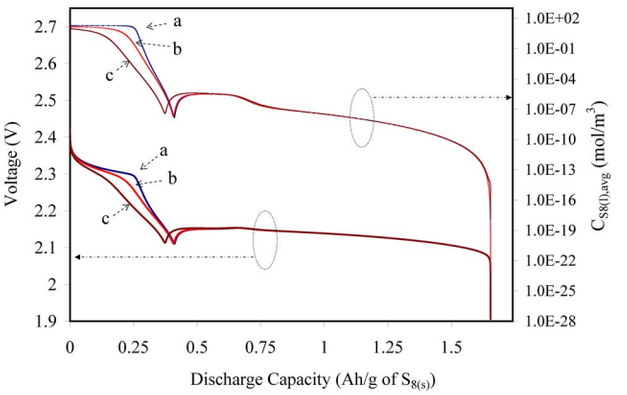

Figure 6. (Color online) Discharge voltage and corresponding average $S_{8(l)}$ concentration profiles for different rates of $S_{8(s)}$ dissolution reaction: (a) k_{S_8} = 1.0 s^{-1}, (b) k_{S_8} = 0.075 s^{-1}, and (c) k_{S_8} = 0.025 s^{-1}.

The predicted voltage profile for cell (V) presented in Fig. 5 shows the ability of the model to "qualitatively" predict all of the characteristics of a typical experimental discharge profile (Fig. 1). (No attempt has been made to do a quantitative comparison between the experimental and simulated discharge profiles.) These characteristics can be further understood by using the average concentration profiles presented in Fig. 4. The voltage of the cell depends on the OCPs of cathodic and anodic reactions which, in turn, depend on the concentrations of reactive species through the Nernst equations. Figure 5 includes the average OCPs of Li/Li$^+$ (Eq. 1) and S_2^{2-}/S^{2-} (Eq. 6) and the average OCP of the full cell ($V_{oc,avg} = U_{6,avg} - U_{1,avg}$). The average OCPs of individual reactions ($U_{1,avg}$ and $U_{6,avg}$) are calculated using the following Nernst equations

$$U_{1,avg} = U_1^{\theta} + \frac{RT}{F}\ln(C_{1,avg}) \quad [41]$$

$$U_{6,avg} = U_6^{\theta} + \frac{RT}{2F}\ln\left(\frac{C_{6,avg}}{C_{7,avg}^2}\right) \quad [42]$$

The average concentrations used in the above equations are the same as those presented in Fig. 4. The average OCP profile of any of the five cathodic reactions can be used to calculate the $V_{oc,avg}$ profile. As the S_2^{2-}/S^{2-} reaction is predominant for a major part of discharge time, it is chosen here for illustration purposes. Because the value of $U_{6,avg}$ and its variation with time is significantly larger than that of $U_{1,avg}$, the shape of the average OCP profile of the cell ($V_{oc,avg}$) closely resembles that of the $U_{6,avg}$. The extra voltage drop seen in the predicted cell voltage profile (V) when compared to the $V_{oc,avg}$ profile can be attributed to the following two factors: (*i*) kinetic overpotential arising from slow cathodic reactions, especially that of S_4^{2-}/S_2^{2-} and S_2^{2-}/S^{2-}, and (*ii*) the $V_{oc,avg}$ profile calculated using the average concentrations in the cathode region, ignoring the variation of concentration gradient across the separator. As there is no precipitation reaction during part I of the discharge, the resulting variations in the concentrations of sulfide ions cause a steep decrease in $V_{oc,avg}$. During the second part of the discharge, the kinetically controlled $Li_2S_{(s)}$ precipitation reaction keeps the variations of the S^{2-} concentration small and hence the change in $V_{oc,avg}$ relatively lower when compared to that in part I of the discharge. The voltage minimum between the two distinct parts of the $V_{oc,avg}$ profile can be attributed to the slow rate of precipitation of $Li_2S_{(s)}$ and the resulting increase in the concentration of S^{2-} to a maximum (critical supersaturation) value.

Next, the model is used to analyze the effect of the $S_{8(s)}$ dissolution reaction rate constant (k_{S_8}) and the rate constant of $Li_2S_{2(s)}$ precipitation reaction ($k_{Li_2S_{2(s)}}$) on the shape of the discharge profile.

Rate constant of $S_{8(s)}$ dissolution reaction (k_{S_8}).— The discharge profiles (at 0.394 A/m^2) obtained with three different values for the rate constant of $S_{8(s)}$ dissolution reaction are presented in Fig. 6. The averaged concentration vs time profiles corresponding to each of the three discharge profiles are also presented on the same graph. When the rate of dissolution is high enough (curve a, k_{S_8} = 1.0 s^{-1}), it replenishes the elemental sulfur in the electrolyte ($S_{8(l)}$) that is being lost due to the electrochemical reduction to S_8^{2-}. As a result, the concentration of $S_{8(l)}$ remains constant until the entire elemental sulfur in the solid state ($S_{8(s)}$) is dissolved completely. The decrease in the OCP of $S_{8(l)}/S_8^{2-}$ reaction for this case is only due to the increasing S_8^{2-} concentration. So, the cell voltage decreases slowly with the discharge. But, for lower rates of $S_{8(s)}$ dissolution (curves b and c), the $S_{8(l)}$ concentration decreases faster with discharge. The drop in OCP of $S_{8(l)}/S_8^{2-}$ reaction in these cases is due to both the increasing S_8^{2-} concentration and the decreasing $S_{8(l)}$ concentration. So, the discharge profile of the cell becomes steeper, causing the formation of S^{2-} and hence the precipitation of $Li_2S_{(s)}$ earlier.

Rate constant of $Li_2S_{2(s)}$ precipitation reaction ($k_{Li_2S_{2(s)}}$).— Both S_2^{2-} and S^{2-} that are being produced during part II of the discharge are only sparingly soluble in the electrolyte. So, the rate constants of the precipitation of $Li_2S_{2(s)}$ and $Li_2S_{(s)}$ decide the amount of each precipitate formed and hence the discharge capacity obtained. For example, Fig. 7 compares the discharge profiles obtained for two different values of $k_{Li_2S_{2(s)}}$. For the case of faster $Li_2S_{2(s)}$ precipitation reaction (curve b, $k_{Li_2S_{2(s)}}$ = 0.05 s^{-1}), some of the S_2^{2-} ions produced are precipitated as $Li_2S_{2(s)}$. These S_2^{2-} ions are not available for further reduction to S^{2-}, and hence the discharge capacity is decreased. The premature end of discharge is also shown by the comparison between the average volume fractions of $Li_2S_{(s)}$ in the cathode for the two cases (Fig.7).

Conclusions

A mathematical model of a lithium–sulfur cell is presented which can be used to predict the variation of the concentration of various species, porosity of the separator and cathode, and the volume fractions of the different precipitates as a function of time and space. Analysis of the average concentrations of various species reveals the

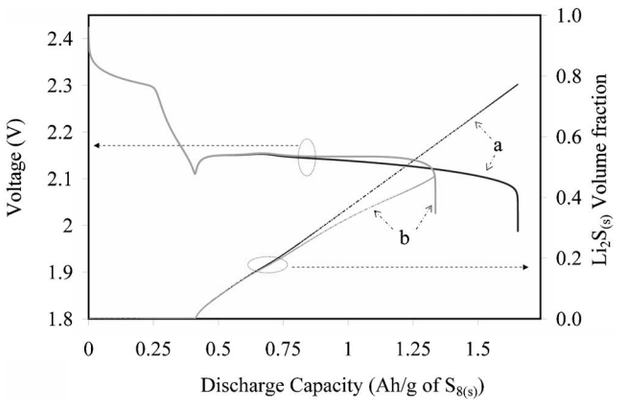

Figure 7. Discharge voltage and corresponding average $Li_2S_{(s)}$ volume fraction profiles for different rates of $Li_2S_{2(s)}$ precipitation: (a) $k_{Li_2S_{2(s)}} = 9.98 \times 10^{-4}$ s^{-1} and (b) $k_{Li_2S_{2(s)}} = 0.05$ s^{-1}.

phenomenological reasons behind the two characteristic stages and the local minimum observed in the experimental discharge profile of a Li/S cell.

Acknowledgment

The financial support for this work provided by Sion Power Corporation, Tucson, Arizona is gratefully acknowledged.

University of South Carolina assisted in meeting the publication costs of this article.

List of Symbols

a	Specific surface area of cathode, m^2/m^3
a_o	Initial value of a, m^2/m^3
b	Bruggeman coefficient
C_i	Concentration of species i, mol/m^3
$C_{i,ref}$	Reference concentration of species i, mol/m^3
$C_{i,avg}$	Average concentration of species i in the cathode, mol/m^3
$D_{i,o}$	Diffusion coefficient of species i in the bulk medium, m^2 s^{-1}
D_i	Diffusion coefficient of species i in the porous medium, m^2 s^{-1}
F	Faraday constant, C/equi
i_j	Current density due to reaction j, A/m^2
$i_{o,jref}$	Exchange current density of electrochemical reaction j at reference concentrations, A/m^2
i_e	Superficial current density in the liquid phase, A/m^2
i_s	Superficial current density in the solid phase, A/m^2
I_{app}	Applied current density, A/m^2
$K_{sp,k}$	Solubility product of precipitate k, units vary, see Table V
k_k	Rate constant of precipitate k, units vary, see Table V
L_s	Thickness of the separator, m
L	Thickness of the cell, m
N_i	Superficial flux of species i, mol m^2 s^{-1}
n_j	Number of electrons transferred in electrochemical reaction j
$p_{i,j}$	Anodic reaction order of species i in electrochemical reaction j
$q_{i,j}$	Cathodic reaction order of species i in electrochemical reaction j
R	Gas constant, J mol^{-1} K^{-1}
R_i	Production rate of species i due to precipitation reactions, mol m^3 s^{-1}
R'_k	Rate of precipitation of solid species k, mol m^3 s^{-1}
r_i	Production rate of species i due to electrochemical reactions, mol m^3 s^{-1}
$s_{i,j}$	Stoichiometric coefficient of species i in electrochemical reaction j
T	Temperature, K
t	Time, s
U_j^θ	Standard OCP of electrochemical reaction j, V
$U_{j,ref}$	OCP of electrochemical reaction j at reference concentrations, V
$U_{j,avg}$	Average OCP of electrochemical reaction j calculated at average concentrations, V
$\tilde{V}_k$	Molar volume of the precipitate k, m^3/mol
$V_{oc,avg}$	Average open-circuit voltage of the cell, V
z_i	Charge number of species i

Greek symbols

α_{aj}	Anodic transfer coefficient of reaction j
α_{cj}	Cathodic transfer coefficient of reaction j
ε	Porosity of separator and cathode
ε_k	Volume fraction of precipitate k in the separator and cathode
ϕ_1	Potential in the solid phase, V
ϕ_2	Potential in the liquid phase, V
$\gamma_{i,k}$	Number of ionic species i produced by dissociation of precipitate k
η_j	Overpotential for electrochemical reaction j
σ	Effective conductivity of solid phase of the cathode, S/m
ξ	Morphology parameter

References

1. M. V. Merrit and D. T. Sawyer, *Inorg. Chem.*, **9**, 211 (1969).
2. H. Yamin, A. Gorenshtein, J. Penciner, Y. Sternberg, and E. Peled, *J. Electrochem. Soc.*, **135**, 1045 (1988).
3. R. D. Rauh, K. M. Abraham, G. F. Pearson, J. K. Sruprenant, and S. B. Brummer, *J. Electrochem. Soc.*, **126**, 523 (1979).
4. E. Peled, Y. Sternberg, A. Gorenshtein, and Y. Lavi, *J. Electrochem. Soc.*, **136**, 1621 (1989).
5. J. Shim, K. A. Striebel, and E. J. Cairns, *J. Electrochem. Soc.*, **149**, A1321 (2002).
6. S. Cheon, K. Ko, J. Cho, S. Kim, E. Chin, and H. Kim, *J. Electrochem. Soc.*, **150**, A796 (2003).
7. Y. Mikhaylik and J. R. Akridge, *J. Electrochem. Soc.*, **151**, A1969 (2004).
8. M.-Y. Chu, L. C. De Jonghe, S. J. Visco, and B. D. Katy, U. S. Pat. 6,030,720 (2000).
9. J. Newman and K. E. Thomas-Alyea, *Electrochemical Systems*, 3rd ed. John Wiley & Sons, New York (2004).
10. R. E. White, S. E. Lorimer, and R. Darby, *J. Electrochem. Soc.*, **130**, 1123 (1983).
11. K.-C. Tsaur and R. Pollard, *J. Electrochem. Soc.*, **133**, 2296 (1986).